

Dynamic mode decomposition of geostrophically balanced motions from SWOT Cal/Val in the separated Gulf Stream

T. Uchida^{1,2}✉, B. Yadidya³, K. Lapo⁴, X. Xu², J. Early⁵, B. Arbic³, D. Menemenlis⁶, L. Hiron², E. Chassignet², J. Shriver⁷ & M. Buijsman⁸

¹Moscow Inst. Phys. Tech. (МФТИ), Russia; ²Florida State Univ., USA; ³Univ. Michigan, USA; ⁴Univ. Innsbruck, Austria; ⁵NorthWest Assoc., USA; ⁶San Jose State Univ., USA; ⁷Naval Res. Lab., USA; ⁸Univ. South. Missi., USA

Correspondence to: takachanbo@gmail.com



The decomposition of oceanic flow into its geostrophically balanced and unbalanced motions carries theoretical and practical significance for the oceanographic community. These two motions have distinct dynamical characteristics and affect the transport of tracers differently from one another. The launch of the Surface Water and Ocean Topography (SWOT) satellite provides a prime opportunity to diagnose the surface balanced and unbalanced motions on a global scale at an unprecedented spatial resolution. Here, we apply dynamic-mode decomposition (DMD), a linear-algebraic data-driven method, to tidally-forced idealized and realistic numerical simulations at submesoscale-permitting resolution and SWOT Cal/Val observations of sea-surface height (SSH) in the separated Gulf Stream. DMD can separate out the spatial modes associated with sub-inertial periods from super-inertial periods. The sub-inertial modes of DMD can be used to extract geostrophically balanced motions from SSH fields, which have an imprint of internal gravity waves (IGWs). We utilize the joint probability density function (PDF) of relative vorticity and strain rate as the metric to gauge the extraction of geostrophy.

Dynamic mode decomposition (DMD)

At the basic level, DMD is a method that seeks a locally linear dynamical system

$$\frac{d}{dt}\boldsymbol{\eta} = \mathbf{A}\boldsymbol{\eta}, \quad (1)$$

where \mathbf{A} is a linear operator and approximately encapsulates all physical processes responsible for the system to step forward in time. In discrete form, this can be recasted as

$$\boldsymbol{\eta}_n = \mathbf{A}\boldsymbol{\eta}_{n-1} = \mathbf{A}^n\boldsymbol{\eta}_0, \quad (2)$$

where $\mathbf{A} = \exp(\mathbf{A}\Delta t)$ and $n = 1, 2, \dots$ is the time step. Δt is the time between the time steps when discretizing (1). The goal of DMD is to determine \mathbf{A} so that the solution to (2) can be expressed by the eigenvalues λ and eigenvectors $\boldsymbol{\psi}$ of the discrete-time map \mathbf{A}

$$\boldsymbol{\eta}_n = \sum_{j=1}^r \boldsymbol{\psi}_j \lambda_j^n \mathbf{b}_j, \quad (3)$$

where \mathbf{b}_j are the coordinates of the initial state $\boldsymbol{\eta}_0$ in the eigenvector basis, and r is the rank of singular-value decomposition (SVD) of \mathbf{A} . Equation (2) can be expanded without a loss of generality as

$$\mathbf{H} = \begin{bmatrix} \boldsymbol{\eta}_0 & \boldsymbol{\eta}_1 & \dots & \boldsymbol{\eta}_{n-1} \end{bmatrix}, \quad \mathbf{H}' = \begin{bmatrix} \boldsymbol{\eta}_1 & \boldsymbol{\eta}_2 & \dots & \boldsymbol{\eta}_n \end{bmatrix}, \quad (4)$$

where \mathbf{H} and \mathbf{H}' are shifted by one time step.

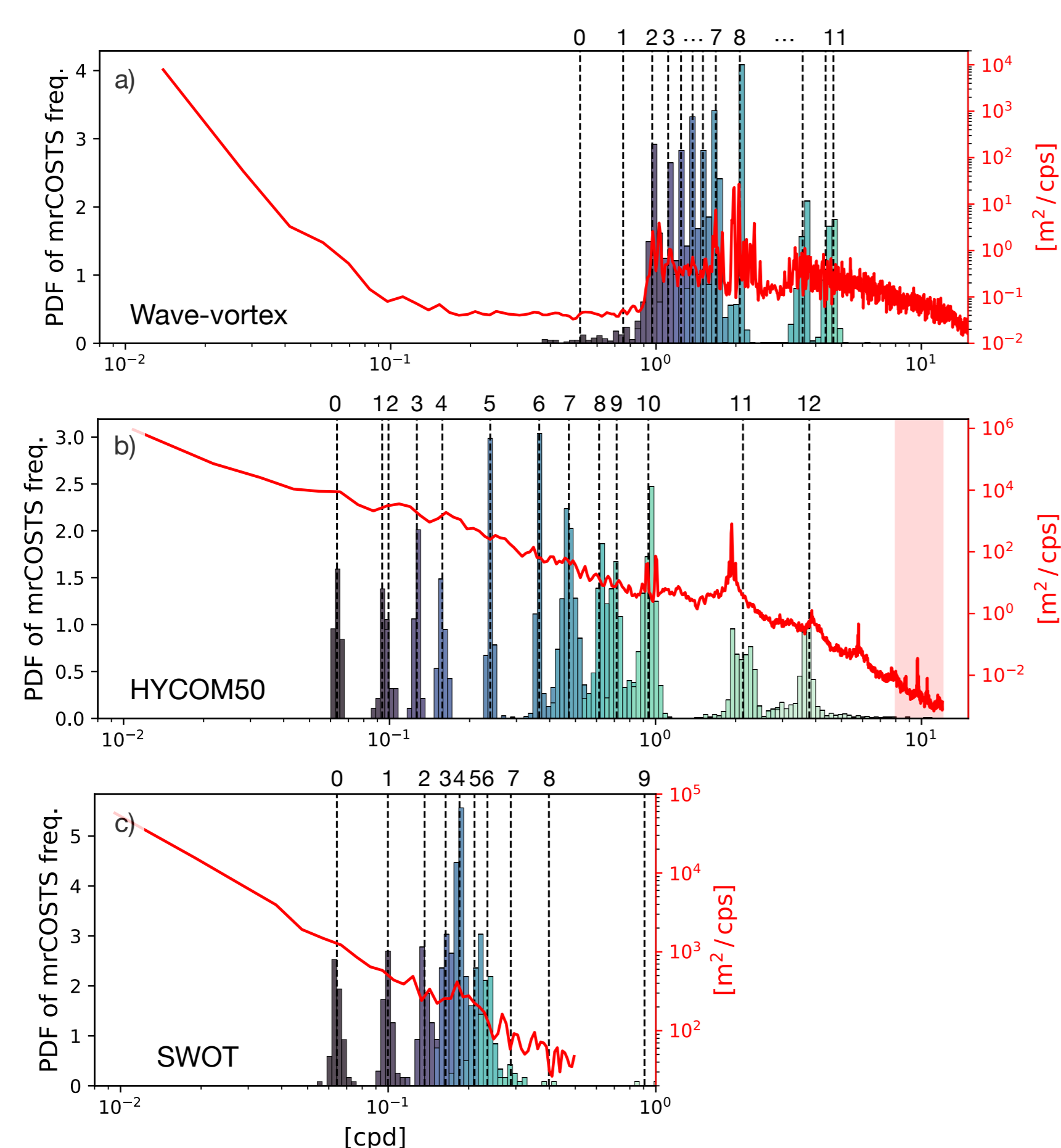
The DMD algorithm produces a low-rank eigen decomposition (3) of matrix \mathbf{A} that optimally minimizes the Frobenius norm $\|\mathbf{H}' - \mathbf{A}\mathbf{H}\|_F$. By rewriting $\omega_j = \ln(\lambda_j)/\Delta t$, the approximate solution for all future times can be predicted as

$$\boldsymbol{\eta}(t, \mathbf{x}) \approx \sum_{j=1}^r \boldsymbol{\psi}_j(\mathbf{x}) \exp[(\Re[\omega_j] + i\Im[\omega_j])t] \mathbf{b}_j. \quad (5)$$

The real part of frequency, $\Re[\omega_j]$ gives growing or decaying modes in time while the imaginary part $\Im[\omega_j]$ corresponds to oscillating modes [4].

The key here is that DMD decomposes the data into spatial modes associated with specific frequencies. We shall exploit the fact that **geostrophic balance should only apply to motions slower than the inertial period**.

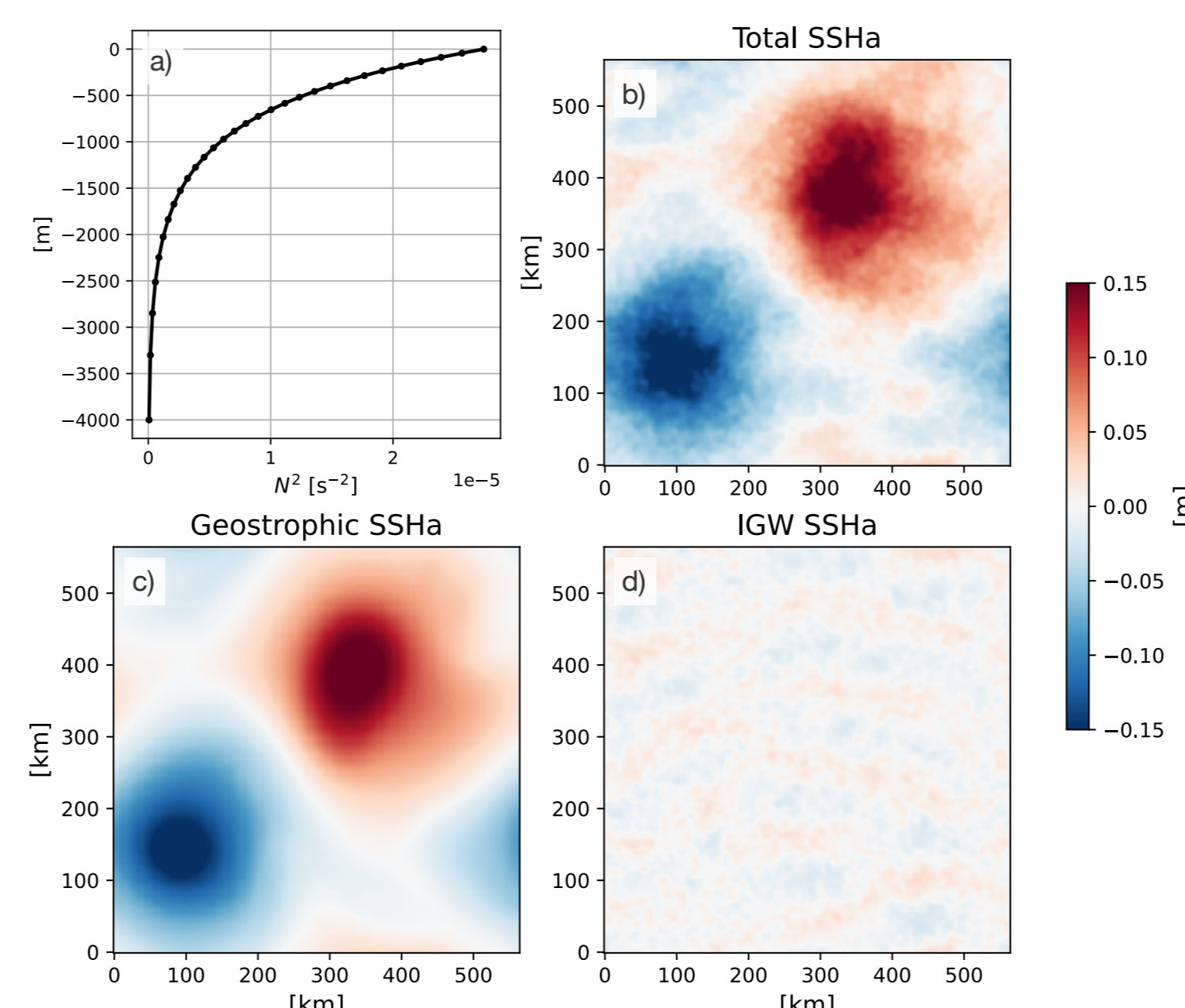
- Geostrophically-balanced dynamics: $|\boldsymbol{\psi} \cdot \mathbf{b}|$ for $\Im[\omega] < |f|$;
- Submesoscale dynamics and IGWs: $|\boldsymbol{\psi} \cdot \mathbf{b}|$ for $\Im[\omega] \gtrsim |f|$.



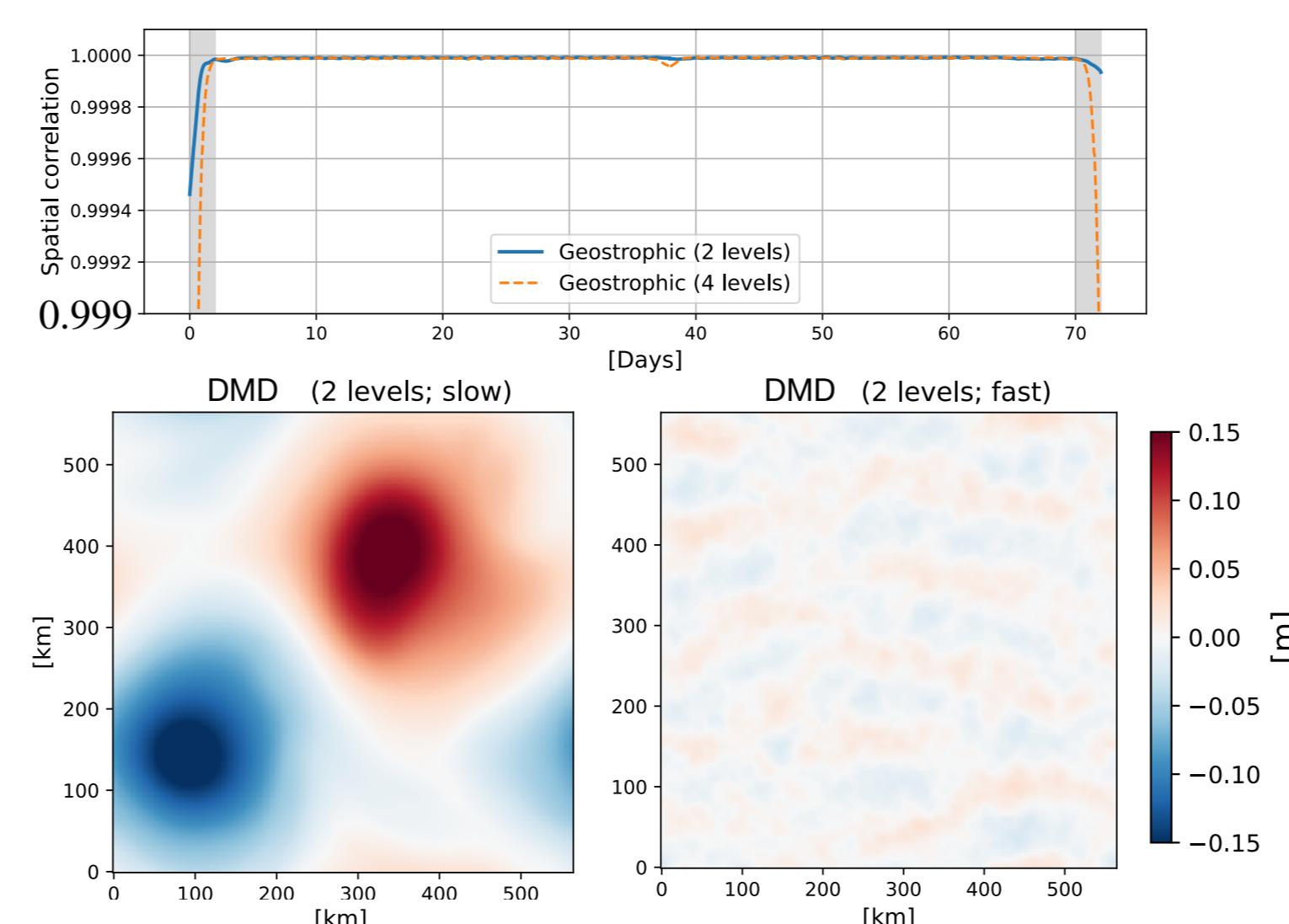
PDF of the DMD-derived frequencies in cycles per day, $\Im[\omega_j]/2\pi$. Wave-vortex case (a), HYCOM50 case (b) and SWOT Cal/Val case (c). Frequency spectra are shown in red curves.

Idealized wave-vortex simulation

An unambiguous decomposition between linear waves and geostrophic motions in arbitrary stratification can be made under flat-bottom boundary conditions by inverting quasi-geostrophic potential vorticity [3]. The eigenmodes from the decomposition form a spectral basis for the wave-vortex model [2], which then solves the equations of motion for a doubly-periodic rotating non-hydrostatic Boussinesq fluid. At each instant in time the complete state of the fluid is decomposed into geostrophic and wave modes, while the non-linear time steps flux energy between modes. We use hourly outputs to construct \mathbf{H} and \mathbf{H}' ($\Delta t = 1$ hour).



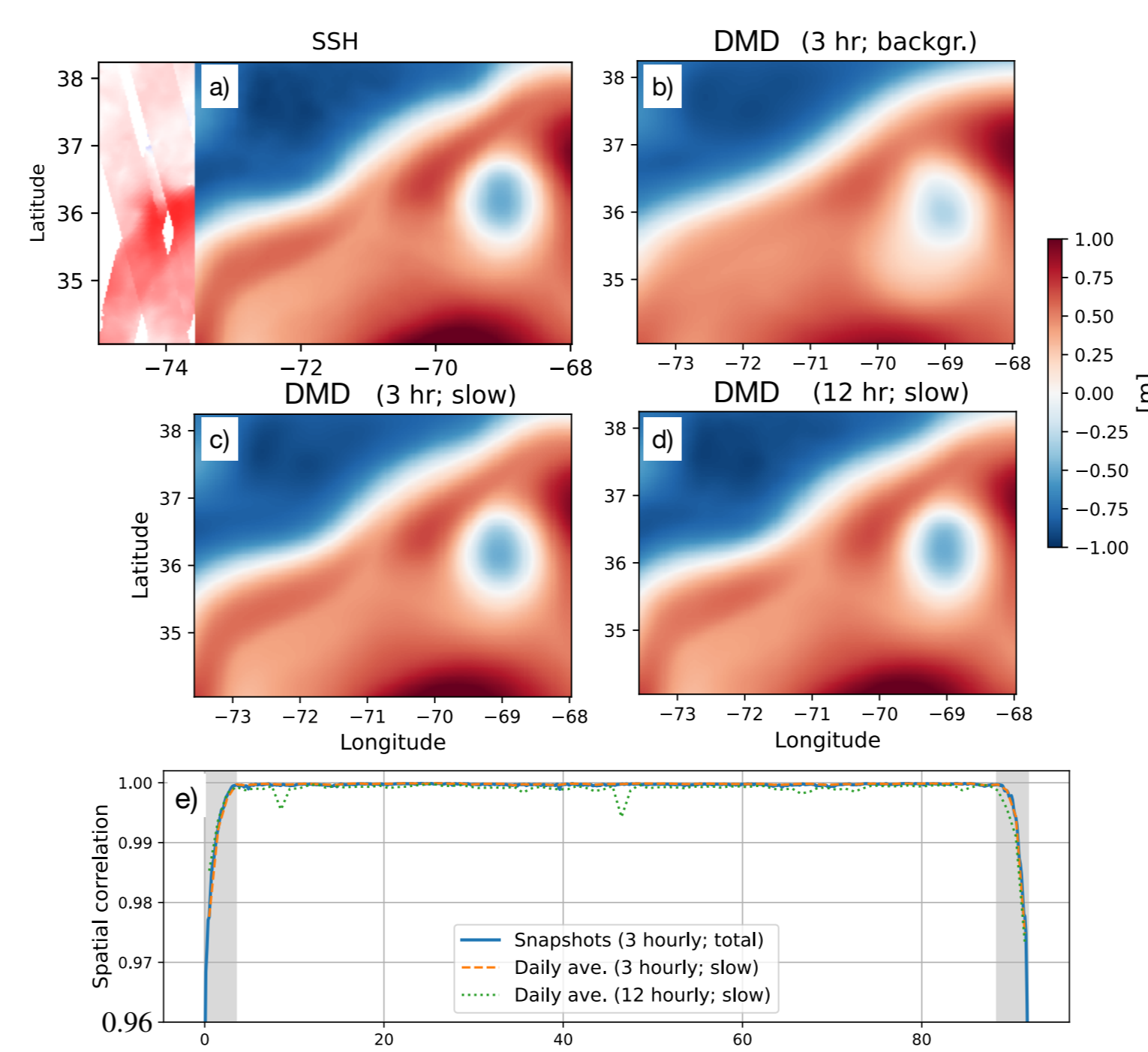
Buoyancy frequency (N^2) with an exponential vertical profile (a) and snapshots of the total SSHa and its geostrophic and IGW components at an arbitrary time step (i.e., the 200th time step after the flow is spun up) from the doubly-periodic wave-vortex simulation (b-d). N^2 is kept stationary throughout the simulation.



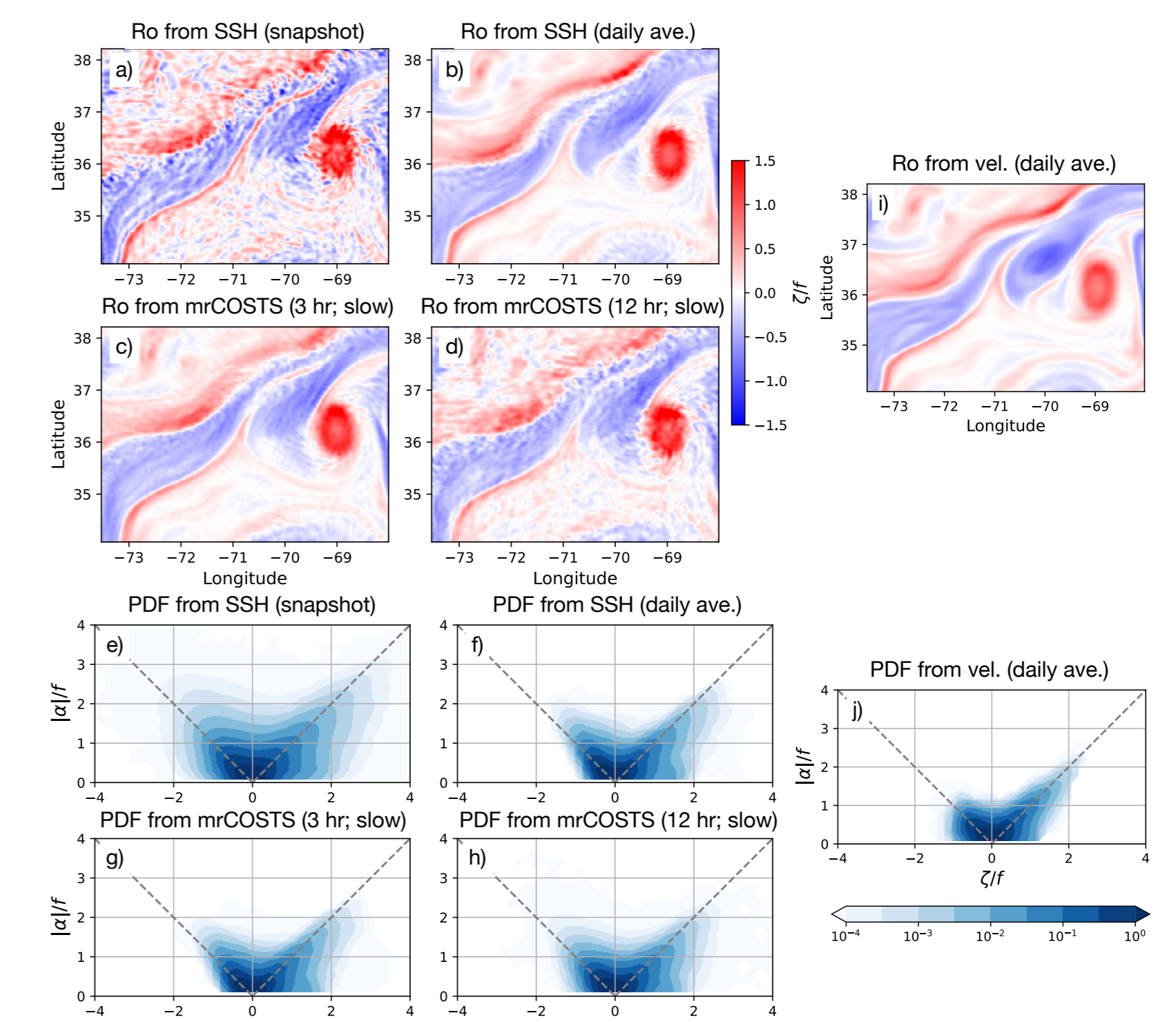
Time series of the spatial correlation between the geostrophic component from the wave-vortex SSH field and DMD reconstruction of the subinertial component (a). The x axis shows the number of days of model simulation. A snapshot of the DMD subinertial component on the same day as in Fig. 2c when DMD is applied (b). The DMD superinertial component (c). The difference between the wave-vortex geostrophic component and DMD subinertial component (d) and between the DMD superinertial component and the IGW component (e).

Tidally-forced realistic submesoscale-permitting simulation (HYCOM50)

We take the hourly averaged SSHa outputs from an atmospherically and tidally forced North Atlantic simulation at $1/50^\circ$ resolution using the HYbrid Coordinate Ocean Model [6]. We construct \mathbf{H} and \mathbf{H}' by taking data every three and 12 hours ($\Delta t = 3, 12$ hours) during the months of August–October, 2003.



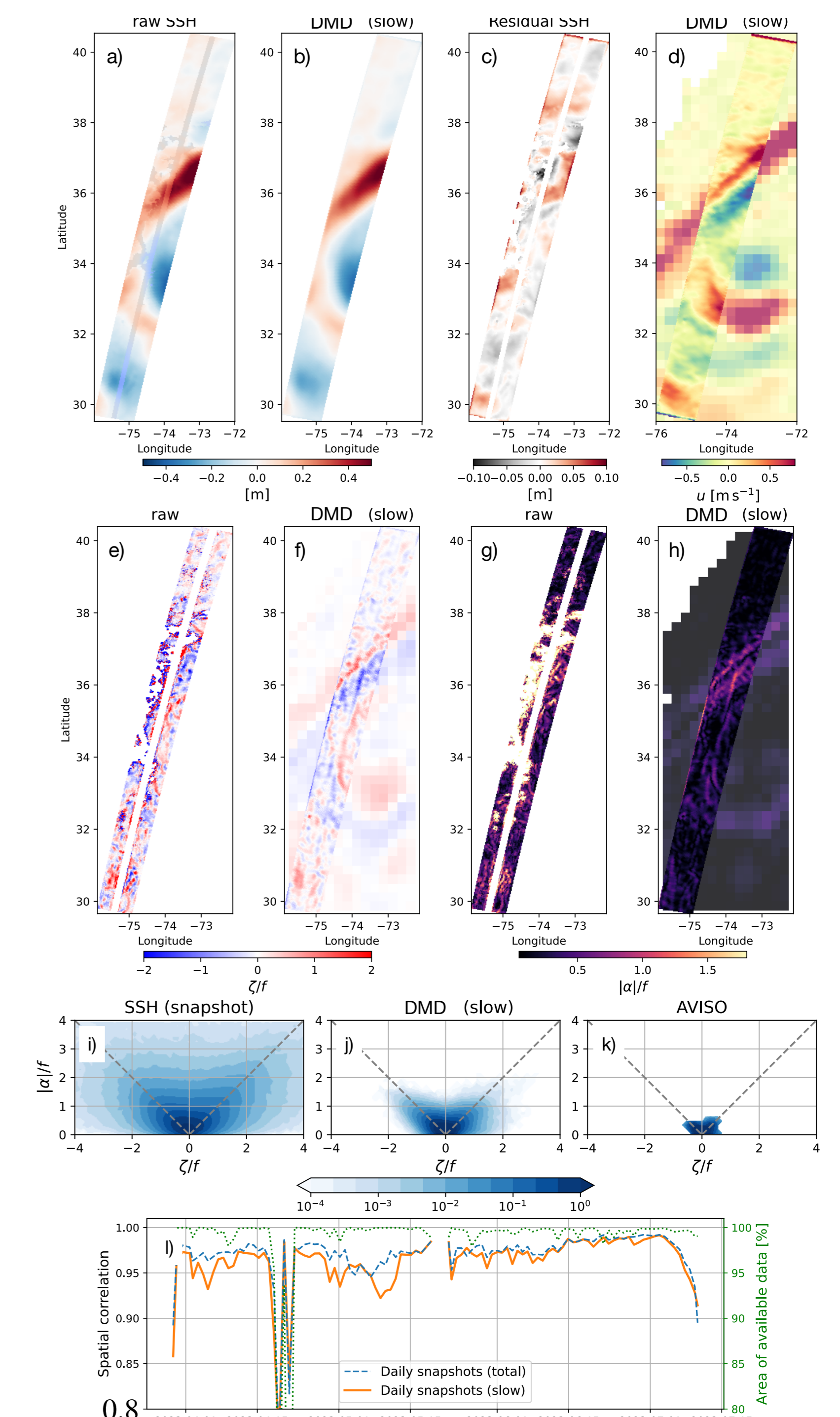
Instantaneous snapshots of SSHa and its DMD reconstruction on an arbitrary day. HYCOM50 output of instantaneous SSHa spatially smoothed using a Gaussian filter with a standard deviation of 10 km (a), the slowest (background) DMD band where SSHa fields were fed three hourly (b), and DMD extraction of sub-inertial component (c). DMD extraction of the sub-inertial component where SSHa fields were fed 12 hourly (d). Time series of spatial correlation between SSHa and DMD reconstructions (e).



Spatial maps of relative vorticity normalized by the local Coriolis frequency ζ/f , viz. the local Rossby number Ro from HYCOM50. Panel (a) shows Ro diagnosed from an instantaneous SSHa field spatially smoothed using a Gaussian filter with a standard deviation of 10 km, and when the hourly SSHa fields are daily averaged to diagnose Ro (b). Instantaneous DMD reconstructions of the subinertial component of Ro when data are fed every three and 12 hours (c, d). Joint PDFs of Ro and strain rates $|\alpha|/f$ normalized by f for each case over the three months of August–October (e–h). A spatial map of Ro and joint PDF of Ro and strain rate at the surface computed from daily-averaged and spatially-smoothed total velocity using a Gaussian filter with a standard deviation of 10 km is shown for reference (i, j).

SWOT Cal/Val (2 km, version 1.0)

We use pass number nine between 30° – 40° N and 284° – 288° E, situated across the separated Gulf Stream path [1] ($\Delta t = 24$ hours).



L3 SWOT observation of SSHa on June 21, 2023 (a), DMD reconstruction of the slow component of the spatially filtered SSHa (b), and the difference between the two (c). Zonal geostrophic velocity diagnosed from the DMD subinertial component (d). ζ/f and $|\alpha|/f$ diagnosed from the SWOT data and DMD subinertial component (e–h). Results from daily-averaged 0.25° gridded AVISO are shown in lighter shadings in contrast to DMD. Joint PDF of ζ/f and $|\alpha|/f$ diagnosed from raw SWOT data, DMD subinertial component and AVISO during April–June, 2023 (i–k). Time series of spatial correlation between SWOT SSHa and its DMD reconstructions (l). The dashed blue curve documents the correlation between instantaneous SSHa and total DMD reconstruction. The orange-solid curve shows the correlation between SSHa and DMD subinertial component.

References

- [1] G. Dibarboure, C. Anadon, F. Briol, R. Chevrier, et al. Blending 2D topography images from SWOT into the altimeter constellation with the Level-3 multi-mission DUACS system. *Ocean Sci.*, 2024.
- [2] J. J. Early, B. Avila, L. Fabre-Lima, and M. A. Sundermeyer. Energy-Pathways-Group/GLCOceanKit: Pre-release of the non-hydrostatic wave-vortex model [Software], 2024.
- [3] J. J. Early, M. P. Lelong, and M. A. Sundermeyer. A generalized wave-vortex decomposition for rotating Boussinesq flows with arbitrary stratification. *J. Fluid Mech.*, 912:A32, 2021.
- [4] K. Lapo, S. M. Ichimaga, and J. N. Kutz. A method for unsupervised learning of coherent spatiotemporal patterns in multiscale data. *Proc. Nat. Acad. Sci.*, 122(7):e2415786122, 2025.
- [5] T. Uchida, B. Yadidya, K. E. Lapo, X. Xu, et al. Dynamic mode decomposition of geostrophically balanced motions from SWOT Cal/Val in the separated Gulf Stream. *Earth Space Sci.*, 12(8):e2024EA004079, 2025.
- [6] X. Xu, E. Chassignet, A. Wallcraft, B. Arbic, et al. On the spatial variability of the mesoscale sea surface height wavenumber spectra in the Atlantic Ocean. *J. Geophys. Res.: Oceans*, 127(10):C2023JC018769, 2022.